Met. Mater. Int., Vol. 16, No. 5 (2010), pp. 709~716
doi: 10.1007/s12540-010-1003-x Published 26 October 2010

Tensile Properties and Fracture Characteristics of ECAP-Processed Al and Al-Cu Alloys

Mohamed Ibrahim Abd El Aal[1,3], Nahed El Mahallawy[2], Farouk A. Shehata[1], Mohamed Abd El Hameed[1], Eun Yoo Yoon[3], Jung Hwan Lee[4], and Hyoung Seop Kim[3,*]

[1]Mechanical Design and Production Department, Faculty of Engineering, Zagazig University, Zagazig, Egypt
[2]Faculty of Engineering and Material Science, German University in Cairo, Egypt
[3]Department of Materials Science and Engineering, POSTECH (Pohang University of Science and Technology), Pohang-si, Gyeongbuk 790-784, Korea
[4]Korea Institute of Materials Science (KIMS), Changwon-si, Gyeongnam 641-831, Korea

(received date: 5 October 2009 / accepted date: 22 February 2010)

In the present paper, billets of pure Al, and cast-homogenized Al-2 wt.%, 3 wt.%, and 5 wt.% Cu alloys were successfully processed by equal channel angular pressing (ECAP) up to 10 passes without fracture at room temperature using a die with a channel angle of 110°. Giant strains imposed on workpieces lead to extreme dislocation densities, microstructural refinement, and finally ultrafine grained materials. Tensile tests were employed to examine the fracture modes and fracture surface morphologies of the ECAP-processed Al and Al-Cu alloy samples. In particular, the effects of the number of ECAP passes and the Cu content were investigated.

Keywords: equal channel angular pressing, severe plastic deformation, Al, Al-Cu alloy, fracture mode

1. INTRODUCTION

Al-Cu cast alloys are among the most important Al alloys widely used in the aerospace industry owing to their light weight. However, due to their poor mechanical properties in as-cast conditions, their mechanical properties must be improved through various thermo-mechanical processes, e.g., heat treatment processing such as aging and solution treatments.

During the last decade, metallic materials with nanometer-[1-3] or ultrafine submicrometer-sized grains after severe plastic deformation (SPD) processing have received a considerable amount of attention due to their unique mechanical and physical properties and high performance capabilities [4-6]. Equal channel angular pressing (ECAP) is considered as the most popular and potential methods among various SPD processes. The principle of ECAP and the properties of the ECAP-processed materials have been discussed by many researchers [7-16].

Recently, it was found that ECAP without any aging treatment improves the mechanical properties of Al-Cu alloys. The microstructure and hardness of Al-1.7 wt.% Cu alloy after ECAP [17] as well as the cyclic deformation and fatigue properties of Al-0.7 wt.% Cu alloy [18], the shear feature of Al-33 wt.% Cu eutectic alloy processed at 400 °C [19], the tensile properties and fracture modes of cast Al-0.63 wt.% Cu and Al-3.9 wt.% Cu alloys [20] subjected to ECAP were studied. Recently, Prados *et al.* investigated the tensile behavior of an ECAP-processed Al-4 wt.% Cu alloy [21]. However, information related to the fracture characteristics of the ECAP-processed Al-Cu alloys remains scarce.

In the present paper, the effects of the Cu content up to 5 wt.% in Al-Cu alloys and the effects of the number of ECAP passes on the tensile properties, in particular, the fracture characteristics of ECAP-processed samples are investigated.

2. EXPERIMENTAL PROCEDURE

Al-Cu alloys with 2 wt.%, 3 wt.% and 5 wt.% Cu contents were manufactured by a casting route and then homogenization treated at 550 °C for 7 days. Commercially pure Al ingots were also used for comparison. The samples were

*Corresponding author: hskim@postech.ac.kr

machined to 15 mm in diameter and 80 mm in length for ECAP. A split-type ECAP die was fabricated with a channel angle of 110° and an outer corner angle of 15°. This die geometry (channel angle and corner angle) generates an average strain of 0.77 for each pass, calculated from the Iwahashi equation [8]. The preform samples were well lubricated with zinc stearate between each pass. ECAP of the samples was processed via route A at room temperature up to 8, 9, and 10 passes for Al, Al-2 wt.% Cu, and both Al-3 wt.% and 5 wt.% Cu, respectively.

Cylindrical tensile specimens 5 mm in diameter with a gauge length of 20 mm were machined from the ECAP-processed samples with the axis of tensile test parallel to the pressing direction. The tensile tests were conducted until failure at room temperature using a TESTO METRIC 200KN universal tensile machine operating at a constant initial strain rate of 8.33×10^{-3} s^{-1}. The tensile tests were repeated three times for each condition, and the average value was taken for the analyses. The fracture surface modes and morphology of the tensile testing specimens were then investigated using JEOL JSM 5410-Scanning electron microscopy (SEM) operating at 15 kV. A three-dimensional total analysis system (Dual Beam FIB) equipped with electron backscattered diffraction (EBSD, Link EDAX system) and associated software (OIM ver. 4.5) was used to characterize the statistical variations of the grain size and the misorientation angle. It was also used to determine the average grain sizes and misorientation angles. The step size for EBSD mapping was 60 nm. The samples for the EBSD study were examined on the cross-sectional plane parallel to the extrusion (longitudinal) direction.

3. RESULTS AND DISCUSSION

3.1. Tensile properties of the ECAP-processed Al and Al-Cu alloys

The effect of the number of ECAP passes on the tensile properties (ultimate tensile stress: UTS, 0.2 % offset proof stress and elongation) of pure Al and Al-Cu alloys is shown in Fig. 1. It was observed that the UTS in Fig. 1(a) and proof stress in Fig. 1(b) increased, while the elongation in Fig. 1(c) decreased with the number of ECAP passes. The increase in strength in these materials is attributed to the grain refinement, as observed in previous work [22]. The application of ECAP to Al allows up to 10 passes before fracture, where a high strength value of 189 MPa was obtained. However, the elongation of Al was reduced from the initial 56 % to 21 % after 10 passes of ECAP. It was reported that route A ECAP resulted in higher elongation than route C in the case of pure Al [23].

The UTS after 2 passes increased by 257 %, 261 %, and 236 % in the Al-2 %, 3 %, and 5 % Cu alloys, respectively. The UTS values continued to increase with the number of ECAP passes, reaching 363 MPa, 446 MPa, and 493 MPa in Al-2 % Cu after 9 passes, Al-3 % Cu after 8 passes and Al-5 % Cu after 8 passes, respectively. A similar trend was observed in previous work [20,21] involving an Al-Cu alloy with Cu contents of 3.9 % and 4 %, where the UTS values were as low as 290 MPa and 315 MPa, respectively. A similar trend in the 0.2 % offset proof stress was also observed, as shown in Fig. 1(b). The accumulated strain in the material increases with the number of ECAP passes, leading to a greater reduction in the grain size, fragmentation of θ phase particles [22,24], and continuous hardening up to the ECAP pass limits. Explanation of the increased strength and decreased elongation can be obtained through variation of the average grain size and the average misorientation angle, as shown in Figs. 2(a) and (b), respectively. The average grain size in Fig. 2(a) was observed to be 1.7 μm, 0.43 μm and 0.23 μm after 2, 4 and 10 passes, respectively. This decrease in the grain size results in an increase in the strength, UTS and 0.2 % offset proof stress, following the Hall-Petch relationship.

The variation in elongation with the number of ECAP passes in the case of Al and Al-Cu alloys is shown in Fig.

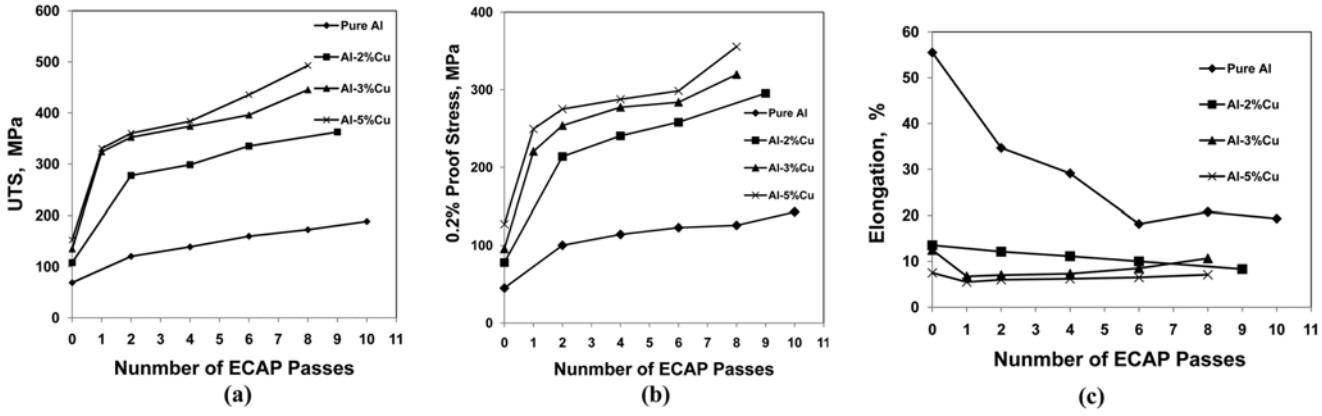

Fig. 1. Dependence of (a) ultimate tensile strength, (b) 0.2% proof stress, and (c) elongation on the ECAP number of passes and copper content for Al-Cu alloys.

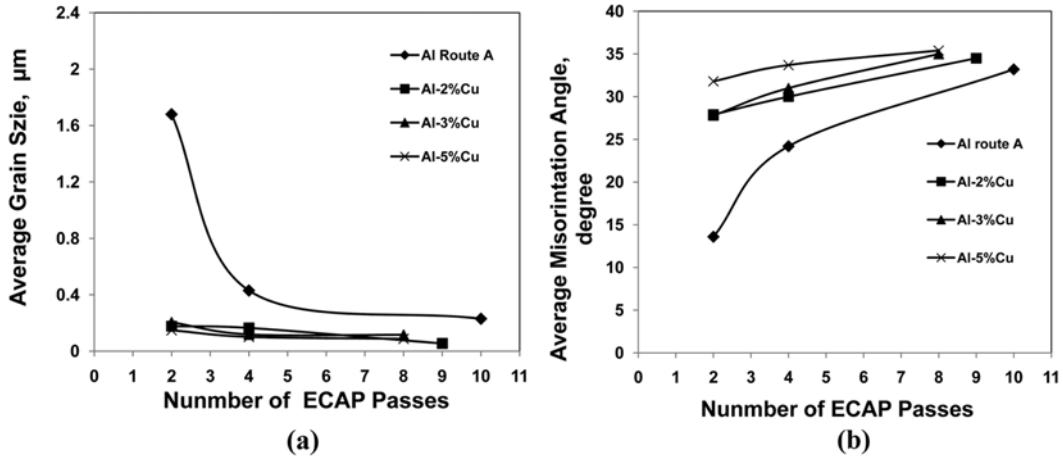

Fig. 2. Variation of (a) the average grain size and the grain boundary misorientation angle of Al and Al-Cu alloys with increasing the ECAP number of passes.

1(c). The elongation decreases with the increase in the number of passes in both pure Al and Al-2 % Cu alloy. However, for a higher Cu content in Al-3 % and 5 % Cu alloys, the elongation decreased after the first pass and then increased gradually with the number of passes, as observed for different Al alloys [25]. The increase in the elongation after the first passes with a higher Cu content in the Al-3 % Cu and 5 % Cu alloys can be explained by the decrease in the size of the second phase θ, which reaches the nano scale with an increase in the imposed strain, as indicated by El Mahallawy *et al.* [22]. The fragmentation of the micro-sized particles and the formation of the nanometer-sized second phase θ particles lead to low deformation resistance and high angle grain boundaries in the deformation zones surrounding the particles [9], i.e., grain boundary evolution from a low to a high angle due to severe deformation [21].

Figure 2(b) shows the variation of the average grain boundary misorientation angle with the increase of the number of passes for different Cu content alloys. It can be observed that the value of the average grain boundary misorientation angle increased with an increase of the number of passes and the Cu content for different Al-Cu alloys. It should be noted that high angle grain boundaries are beneficial to enhance elongation. The change in the elongation with the number of ECAP passes is clear in the Al-Cu alloys, as shown in Fig. 1(c). The Cu content also has a clear effect on the elongation, as in the case of the Al-Cu alloys. The elongation was observed to decrease with an increase in the number of passes for the Al-2 % Cu alloy. It is interesting that for the Al-3 % and 5 % Cu alloys, the elongation was observed to increase after the second pass.

3.2. Fracture mode and fracture surface morphology

Figure 3 shows FE-SEM micrographs of the fractured shapes of the pure Al specimens before and after ECAP up to 10 passes. It can be observed from necking that the mode of fracture in the initial undeformed Al is ductile, as shown in Fig. 3(a). On the other hand, after ECAP of 2 passes and up to 10 passes, the fracture was observed to be a combination of the shear and necking fracture modes. The degree of necking was reduced with the number of ECAP passes due

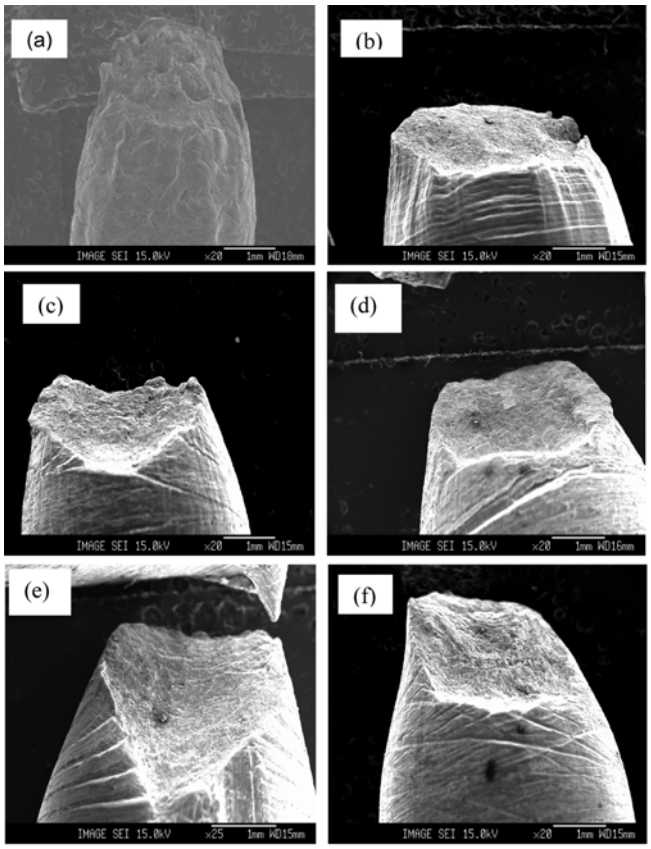

Fig. 3. FE-SEM photomicrograph for fracture modes of Al (a) As-cast, (b) 2 passes, (c) 4 passes, (d) 6 passes, (e) 8 passes, and (f) 10 passes.

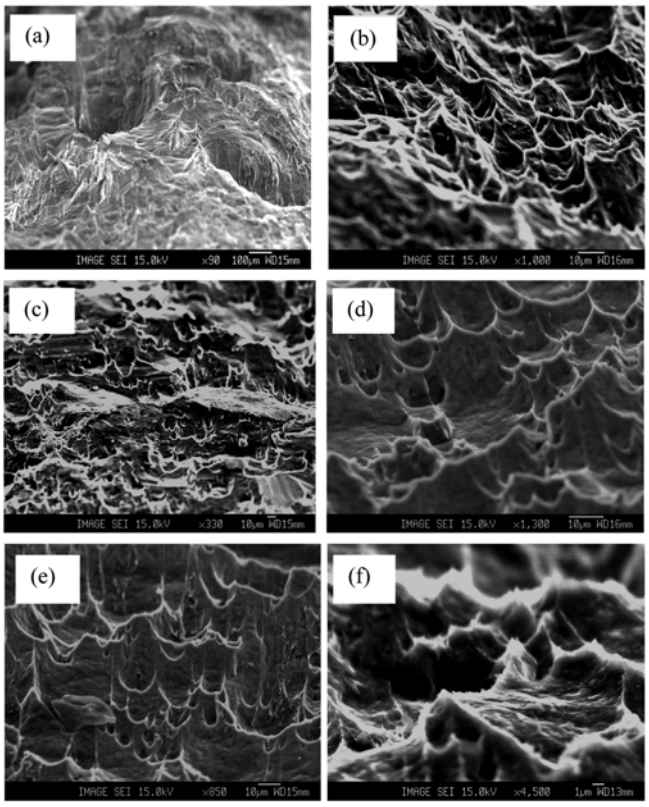

Fig. 4. FE-SEM photomicrograph for fracture surface morphology of Al (a) As-cast, (b) 2 passes, (c) 4 passes, (d) 6 passes, (e) 8 passes, and (f) 10 passes.

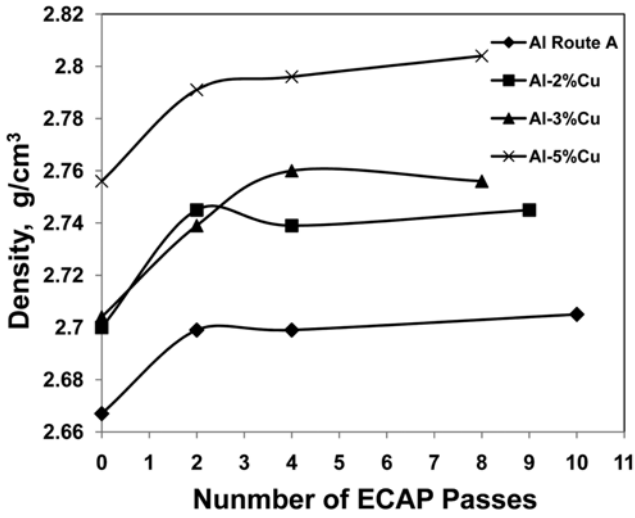

Fig. 5. Density with the increase of the ECAP number of passes for Al a

to the decreasing work-hardening capacity by the work hardening that accumulated during ECAP. The transformation of the fracture mode between routes 1 and 2 can be also explained in terms of the reduction of the grain size. The reduced necking with ECAP coincides with the reduction in the tensile elongation (see Fig. 1(c)).

Figure 4 illustrates the SEM fracture surface morphologies of a pure Al specimen before and after ECAP with different numbers of passes. A large diameter of 176 μm to 180 μm and deep dimples were observed before ECAP, as shown in Fig. 4(a). After ECAP, the dimple sizes decreased and showed a homogeneous distribution across the fracture surfaces. It was also observed that the dimples in the fracture surfaces were shallower than those before ECAP. The average sizes of the dimples in the fracture surfaces decreased to 7.4-5.9 μm, 6.8-2.5 μm, and 3.4-2.4 μm after 2, 4 and 6 passes, respectively, and then became saturated at 3 μm after 8 and 10 passes. The difference in the dimple size is due to the difference in the grain size, which can also be confirmed from the present result, in which the average grain size obtained after 4 passes is very close to the average dimple size of 4.6 μm. A fracture surface full of dimples of different sizes and depths was observed previously in rolling and ECAP-processed commercially pure Al samples tested under different strain rates [26]. The reduction in the diameter and depth of the dimples after increasing the number of ECAP passes is due to a reduction in the work hardenability, which reduces dimple growth after nucleation.

The increase in the density with the number of ECAP passes shown in Fig. 5 contributes to decreasing the dimple size. The dimple size is determined by the initiation size and the number of voids nucleated in the grain boundaries. Hence, the decrease of the void content by complete closeness or a decrease in the void size leads to a decrease of the dimple size. The same behavior of a reduction in the dimple size in the fracture surface was reported in commercially pure Al 1060 processed by ECAP of route Bc up to 2 passes [27].

Figure 6 shows FE-SEM photomicrographs of the Al-2 % specimens before and after ECAP. The brittle fracture modes of the three alloys were observed in the tensile samples before the ECAP process. The fracture in the as-cast sample occurred normal to the tensile axis. After ECAP of the Al-2 % Cu alloy, the fracture mode was the shear mode with a fracture angle of 45° with respect to the tensile axis, as shown in Fig. 6(b). Subsequently, as the number of ECAP passes increased, the fracture continued to show the shear fracture mode with changes in the fracture angles to 41°, 54°, and 42° after 4, 6, and 9 passes, respectively (see Figs. 6(c) to (e)). Hence, the results show that the fracture mode transforms to the shear mode after ECAP. The fracture angles with different numbers of passes were equal or very close to the angle of the maximum shear plane, i.e., 45°. Similar behavior of Al-2 % Cu was observed in the Al-3 % Cu alloy, although this is not shown here. The fracture morphology of the specimen was transformed to the shear morphology with an angle of 53° with respect to the tensile axis. As the num-

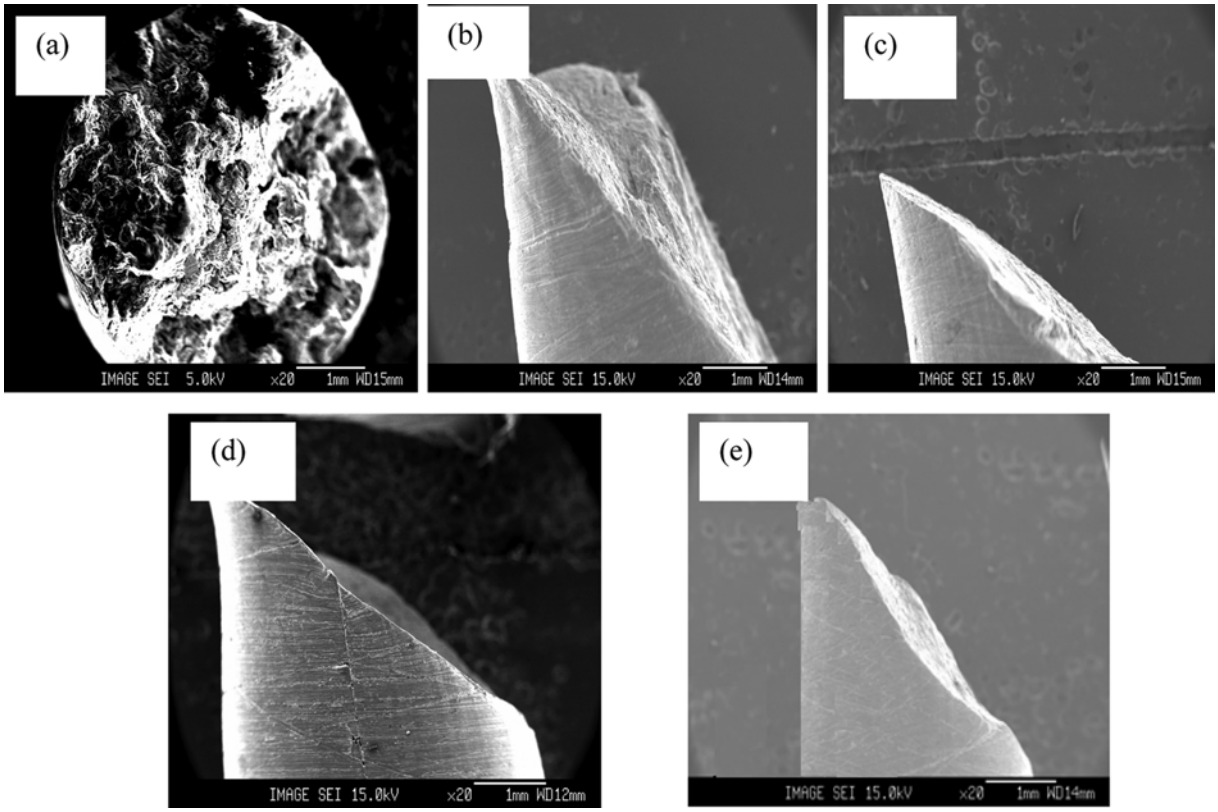

Fig. 6. Fracture morphology of Al-2%Cu alloy. (a) As-cast and ECAP processed up to (b) 2 passes, (c) 4 passes, (d) 6 passes, and (e) 9 passes.

Table 1. The fracture angle of Al-Cu alloys

Alloy	Number of Passes	Fracture angle
Al-2%Cu	2	45
	4	41
	6	54
	9	42
Al-3%Cu	1	53
	2	20
	4	48
	6	50
	8	50
Al-5%Cu	1	53
	2	31
	4	43
	6	45
	8	47

ber of ECAP passes increased, the fracture remained in the shear fracture mode. The fracture angle changed to 20°, 48°, 50° and 50° after 2, 4, 6, and 8 ECAP passes, respectively. After 4 passes, the fracture angle became very close to the value of the angle at 45° of the maximum shear plane. In particular, after 4 passes, the fracture angle was closer to the angle of 45° than that observed in previous work with Al-3.9 % Cu alloy [20]. The same trend continued in the Al-5 % Cu alloy. Table 1 indicates the values of the fracture angles in the different alloys processed with different numbers of ECAP passes. The same fracture mode behavior was also observed in previous work with the Al-Mg alloy [28]. The fracture behavior of the Al-Cu alloys can be explained by the distribution of the hard phase θ along the grain boundaries in the cast alloys before the ECAP process, where the hard phase hindered grain deformation during the tensile tests and therefore made the fracture normal to the load direction. However, the hard phase θ was fragmented and uniformly distributed in the Al matrix during ECAP, as observed in previous work [20,22,24].

Figures 7 and 8 show FE-SEM photomicrographs of the fracture surface morphologies of the Al-2 % Cu alloy specimens before and after ECAP. These figures show that the fracture surface was a brittle mode without dimples in the as-cast samples, which contained dendrite structures. The dendritic structures have average sizes of 65 μm, 60 μm, and 35 μm in the Al-2 %, 3 % Cu, and 5 % Cu alloys, respectively. The same fracture surface features of Al-Cu alloys were observed in previous works with Al-Cu alloy and Al-Zn alloys as the dendrite structures continued to be observed in the fracture surface [21,29]. In the case of ECAP-processed samples, the fracture surfaces were shear fracture surfaces and dendrite

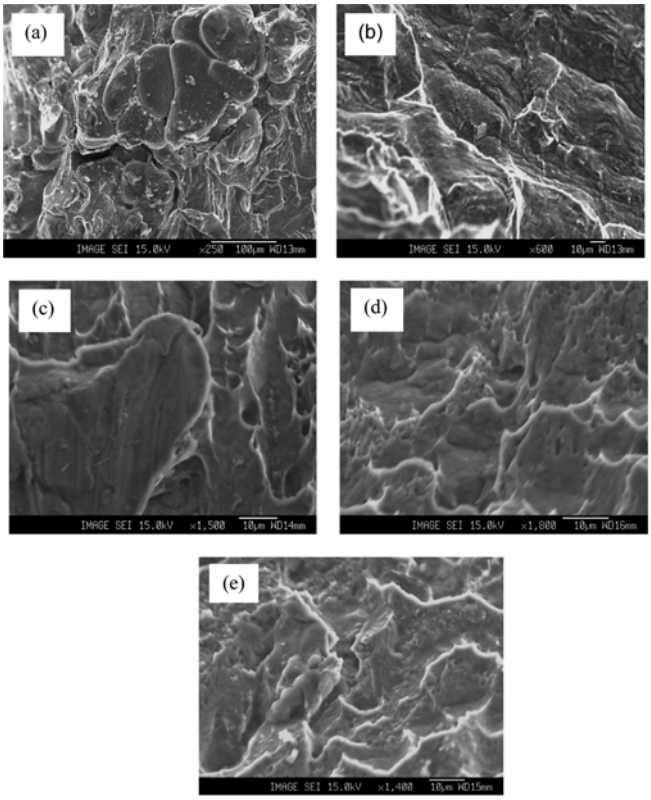

Fig. 7. Fracture surface morphology of Al-2%Cu alloy (a) As-cast and ECAP processed for (b) 2 passes, (c) 4 passes, (d) 6 passes, and (e) 9 passes.

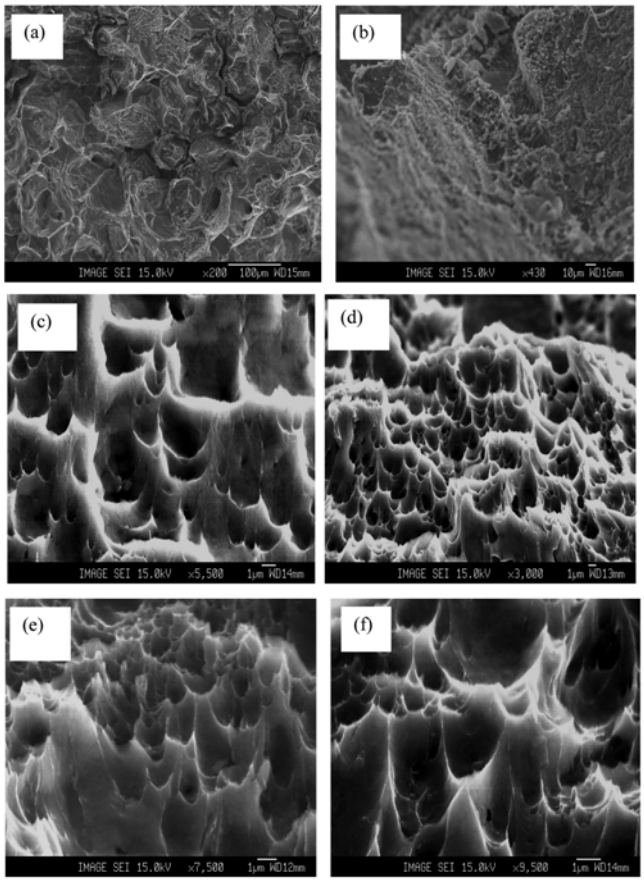

Fig. 8. Fracture surface morphology of Al-3%Cu alloy (a) As-cast and ECAP processed for (b) 1 pass (c) 2 passes, (d) 4 passes, (e) 6 passes, and (f) 8 passes.

structures had completely disappeared from the fracture surface. This was due to SPD during the ECAP process, which leads to grain refinement and a decrease in the work-hardening. As the dendrites were refined and elongated along the shear direction and with further deformation, the grains became fragmented and transformed to an equiaxed structure. The same fracture surface morphology was observed after 4, 6 and 9 passes with the Al-2 % Cu alloy, as shown in Figs. 7(c), (d), and (e), respectively. It should be noted that as the number of ECAP passes increased, shear decohesion and surface cracks appeared on the fracture surface, as the material loses its ductility with grain refinement. The behavior of the fracture surface morphology is consistent with the tensile elongation trend of the Al-2 % Cu alloy, as shown in Fig. 1(c). It can be observed that the elongation decreased with an increase in the ECAP number of passes; this is related to the decrease in the grain size and thus the increase in the strength.

Figure 8 shows the fracture surface morphology of the Al-3 % Cu alloy specimen after ECAP. The fracture surface was observed to be free from the dendrite structure, which completely disappeared from the fracture surface, as shown in Fig. 8(b). This arose due to SPD, which occurred during the ECAP process, leading to grain refinement and strong work-hardening. After 2 passes, the dimples appeared across the fracture surface with an average size of 1.7 μm to 2.1 μm. as shown in Fig. 8(c). As the number of ECAP passes exceeded 4 passes, the number and the homogeneity of the dimples across the fracture surface increased, as shown in Fig. 8(d). The size of the dimples decreased to an average size of 1.4 μm to 1.8 μm in the 4-pass sample. The same fracture surface features also appear with the number of ECAP passes in the 6- and 8-pass samples shown in Figs. 8(e) and (f), respectively. The average size of the dimples decreases as the number of ECAP passes increases, i.e., decreasing to 1.3 μm to 1.4 μm and then to 1.2 μm to 1.4 μm in the 6-pass and 8-pass samples. The same fracture surface characteristics are generally found, in that the dimple size is reduced with the number of ECAP passes during ECAP with the Al-Mg alloy [29], Al-40 % Zn alloy [29] and Ti [30]. This was also observed in the cryorolling process of the Al-Mg-Si alloy [27] with an increase in the thickness reduction ratio. The fracture surfaces in the Al-5 % Cu alloy are similar to those in Al-3 % Cu, although this is not shown here. The difference between the Al-3 % Cu and Al-5 % Cu is in the size of the dimples formed in the fracture surface. The dimple size in the Al-5 %

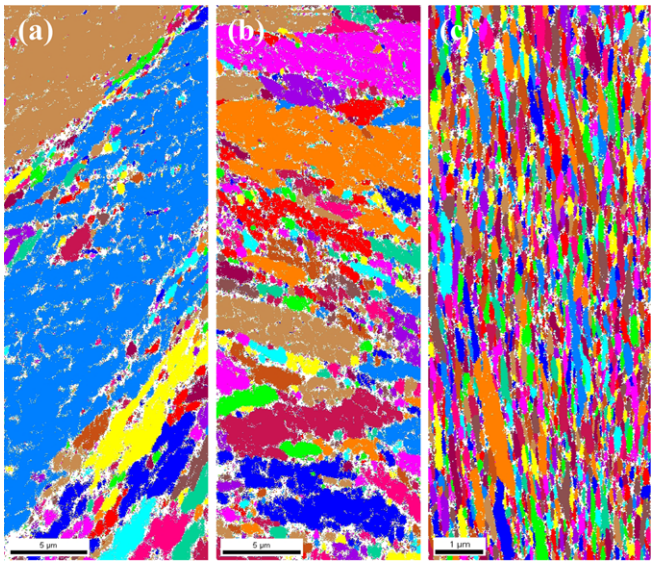

Fig. 9. The EBSD color grain map of Al-2%Cu processed up to (a) 2, (b) 4 and (c) 9 passes.

Cu alloy was smaller than that in the Al-3 % Cu alloy. The average dimple size in Al-5 % Cu was 0.9-1.2, 0.7-1, 0.8-0.9 after 2, 4, 6 and 8 passes, respectively.

This can be explained in terms of the difference in both of the average grain size shown in Fig. 1(a) and the size of the θ phase in both cases [22]. The size of the θ phase in deformed Al-5 % Cu was smaller than that in Al-3 % Cu: The size of the θ phase was approximately 390 nm and 200 nm after 4 and 8 passes, respectively, in Al-5 % Cu. On the other hand, it was 700 nm and 250 nm after 4 and 8 passes, respectively, in Al-3 % Cu, as indicated in previous work [22]. Hence, for both the Al and different Al-Cu samples, it can be concluded that the reduction in the dimple size is related to the decrease in the average grain size and the decrease or closeness of the void in the material during the ECAP process. It should be noted that the dimple size depends on the initiation site and the number of voids that nucleate in the grain boundaries. The closeness and decrease of the void during the ECAP process can be investigated through variation of the density and the void content as the number of passes increases, as shown in Fig. 5, given that it was observed that the density increased for different materials continuously with the increase in the number of passes. The increase in the density can be explained by the decrease in the size or the closeness of the voids. That is, due to the decrease in the void size, the dimple size decreased in the different materials.

Figure 9 shows the sequence of the microstructure evolution in Al-2 % Cu after 2, 4 and 9 passes. The microstructure consists of a combination of elongated and equaxied microstructures after 2 passes. Hence, with the increase in the number of passes to 4 passes, the fraction of the equaxied grains increases across the structure. Finally, after 9 passes, the microstructure completely changes to an approximately equiaxed structure with an average grain size of 55 nm. The same microstructural evolution steps were observed in the Al-3 % and 5 % Cu alloys. These microstructures indicate that after only 2 ECAP passes, the microstructure and therefore the texture of the processed material cause an improvement in the UTS, as shown in Fig. 1(a). The tracing of the elimination of the dendrite structure was also observed during the ECAP processing of Al-40 % Zn and Zn-40 % Al [31,32]. It was also observed that route A is more effective for faster mitigation of the dendrite structure to an equiaxed structure compared to that in the case of route Bc with Al-40 %Zn [31].

4. CONCLUSIONS

In this research, it was possible to use ECAP with Al and Al-Cu (up to 5 wt.% Cu) alloys at room temperature up to 10 passes, corresponding to a total strain of 7.7 with a die channel angle of 110. Tensile tests showed that the ultimate tensile and 0.2 % proof strengths increase with the number of ECAP passes and with the Cu content, while the elongation decreases as the number of ECAP passes increases for both pure Al and Al-2 % Cu alloy. For Al-3 % and 5 % Cu alloys, the elongation decreases after the first ECAP pass and then increases with additional passes due to the breakdown of the hard phase to the nanoscale. The fracture mode and fracture surface morphology were affected by both the ECAP conditions and the Cu content. In pure Al, the fracture mode was transformed from ductile to a combination of the ductile and shear modes as the number of ECAP passes increased. The fracture angles in the Al-Cu alloys were close to or equal to the angle of the maximum shear plane for different Al-Cu alloys, especially after the second pass. The dimple size across the fracture surface decreased remarkably as the number of ECAP passes increased. The same changing behavior in the fracture mode and the fracture surface morphology was observed as both the number of ECAP passes and the Cu content in Al-Cu alloys increased. The decrease of the dimple size was related to the decrease of the grain size and the closeness and reduction of the voids through the ECAP process, leading to an increase in the density.

ACKNOWLEDGMENTS

MAE acknowledges the financial support from the Egyptian Government for his overseas scholarship to conduct research at POSTECH. HSK acknowledges the support of a grant (B551179-08-01-00) from the cooperative research project "Development of common manufacturing technology for high functional susceptor" funded by the Ministry of Knowledge Economy, Republic of Korea.

REFERENCES

1. H. S. Kim, *Scripta mater.* **39**, 1057 (1998).
2. H. S. Kim, C. Suryanarayana, S.-J. Kim, and B. S. Chun, *Powder Metall.* **41**, 217 (1998).
3. H. S. Kim and Y. Estrin, *Appl. Phys. Lett.* **79**, 4115 (2001).
4. R. Z. Valiev, R. K. Islamgalive, and I. V. Alexandrov, *Prog. Mater. Sci.* **45**, 103 (2000).
5. Y. H. Jang, S. S. Kim, S. Z. Han, C. Y. Lim, and M. Goto, *Met. Mater. Int.* **14**, 171 (2008).
6. Y. T. Zhu, T. C. Lowe, and T. G. Langdon, *Scripta mater.* **51**, 825 (2004).
7. V. M. Segal, *Mater. Sci. Eng. A* **197**, 157 (1995).
8. Y. Iwahashi, J. Wang, Z. Horita, M. Nemoto, and T. G. Langdon, *Scripta mater.* **35**, 143 (1996).
9. R. Z. Valiev and T. G. Langdon, *Prog. Mater. Sci.* **51**, 881 (2006).
10. B. S. Moon, H. S. Kim, and S. I. Hong, *Scripta mater.* **46**, 131 (2002).
11. S. C. Baik, Y. Estrin, R. J. Hellmig, H. T. Jeong, H.-G. Brokmeier, and H. S. Kim, *Zeit. Metallkd.* **94**, 1189 (2003).
12. Y. G. Kim, B. C. Hwang, S. H. Lee, C. W. Lee, and D. H. Shin, *J. Kor. Inst. Met. & Mater.* **46**, 545 (2008).
13. Y. G. Kim, Y. G. Ko, D. H. Shin, C. S. Lee, and S. H. Lee, *J. Kor. Inst. Met. & Mater.* **46**, 563 (2008).
14. Y. G. Kim, Y. G. Ko, D. H. Shin, and S. H. Lee, *J. Kor. Inst. Met. & Mater.* **47**, 397 (2009).
15. S. C. Yoon and H. S. Kim, *J. Kor. Inst. Met. & Mater.* **47**, 699 (2009).
16. S. C. Yoon, P. Quang, and H. S. Kim, *J. Kor. Inst. Met. & Mater.* **46**, 144 (2008).
17. M. Murayama, Z. Horita, and K. Hono, *Acta mater.* **49**, 21 (2001).
18. Z. F. Zhang, S. D. Wu, Y. J. Li, S. M. Liu, and Z. G. Wang, *Mater. Sci. Eng. A* **412**, 279 (2005).
19. J. Wang, S. Kang, and H. Kim, *Mater. Sci. Eng. A* **383**, 356 (2004).
20. D. R. Fang, Z. F. Zhang, S. D. Wu, C. X. Huanga, H. Zhang, N. Q. Zha, and J. J. Li, *Mater. Sci. Eng. A* **426**, 305 (2006).
21. E. Prados, V. Sordi, and M. Ferrante, *Mater. Sci. Eng. A* **503**, 68 (2009).
22. N. El Mahallawy, F. A. Shehata, M. A. El Hameed, and M. A. El Aal, *Mater. Sci. Eng. A* **517**, 46 (2009).
23. A. Sivaraman and U. Chakkingal, *J. Mater. Process. Technol.* **202**, 543 (2008).
24. X. X. Chang, L. Z. Yi, L. Y. Tao, D. Peng, and Z. S. Min, *Trans. Nonferrous Met. Soc. China* **108**, 1047 (2008).
25. Z. Horita, T. Fujinami, M. Nemoto, and T. G. Langdon, *J. Mater. Process. Technol.* **117**, 288 (2001).
26. M. Wang and A. Shan, *J. Alloy. Compd.* **455**, L10 (2008).
27. J. W. Wang, Q. Q. Duan, C. X. Huanga, S. D. Wu, and Z. F. Zhang, *Mater. Sci. Eng. A* **496**, 409 (2008).
28. D. R. Fang, Q. Q. Duan, N. Q. Zha, J. J. Li, S. D. Wu, and Z. F. Zhang, *Mater. Sci. Eng. A* **459**, 137 (2007).
29. O. Saray and G. Purcek, *J. Mater. Process. Technol.* **209**, 2483 (2009).
30. Y. G. Ko, D. H. Shin, K. T. Park, and C. S. Lee, *Scripta mater.* **54**, 1785 (2006).
31. G. Purcek, O. Saray, I. Karaman, and T. Kucukomeroglue, *Mater. Sci. Eng. A* **490**, 403 (2008).
32. S. K. Panigrahi and R. Jayaganthan, *Mater. Sci. Eng. A* **480**, 299 (2008).